

# Perforation of thin aluminum alloy plates by blunt projectiles: An experimental and numerical investigation

**G Wei<sup>1</sup> and W Zhang**

Hypervelocity Impact Research Center, Harbin Institute of Technology, Harbin 150001, China

E-mail: weigang.hit@gmail.com

**Abstract.** Reducing the armor weight has become a research focus in terms of armored material. Due to high strength-to-density ratio, aluminum alloy has become a potential light armored material. In this study, both lab-scale ballistic test and finite element simulation were adopted to examine the ballistic resistance of aluminum alloy targets. Blunt high strength steel projectiles with 12.7 mm diameter were launched by light gas gun against 3.3 mm thickness 7A04 aluminum alloy plates at a velocity of 90~170 m/s. The ballistic limit velocity was obtained. Plugging failure and obvious structure deformation of targets were observed. Corresponding 2D finite element simulations were conducted by ABAQUS/EXPLICIT combined with material performance testing. The validity of numerical simulations was verified by comparing with the experimental results. Detailed analysis of the failure modes and characters of the targets were carried out to reveal the target damage mechanism combined with the numerical simulation.

## 1. Introduction

With the requirement of the mobility and flexibility of tanks and armored vehicles in modern local war, reducing the armor weight has become a research focus. Due to high strength-to-density ratio, aluminum alloy has become a potential light armored material [1-4]. Recently, some universities and research institutions have begun to pay attention to the performance of aluminum alloy armor [4-9]. But comparing with large number of public reports about the armor performance of traditional steel armor, aluminum alloy, was investigated relatively less. As a kind of high-strength and lightweight material, 7A04 aluminum alloy has the potential to become armor materials.

In this study, the methods of lab-scale ballistic test and finite element simulation are adopted to examine the ballistic resistance property of 7A04 aluminum alloy targets with thickness 3.3 mm and yield strength 250 MPa against the blunt nose projectiles. The initial velocity versus residual velocity of the projectiles was plotted and the ballistic limit velocity was obtained. Finite element simulation of the impact situation has also been carried out by using an explicit finite element code ABAQUS/Explicit with 2D model. Good agreement between the numerical simulations and the experimental results was found. Detailed analysis of the failure modes and characters of the targets were carried out to reveal the damage mechanism of target combined with the numerical simulation.

<sup>1</sup> Gang Wei, a PhD Candidate at Harbin Institute of Technology, Harbin, China

Email: [weigang.hit@gmail.com](mailto:weigang.hit@gmail.com) Mobile Phone: +86-13674681013

This work is supported by National Nature Science Foundation of China under Grant 11072072



## 2. Experiment set-up and results

### 2.1. Experiment set-up

The impact tests within the velocity range of 90-170 m/s were performed at a one-stage compressed gas gun with a 12.7 mm caliber diameter and 1.2 m length launch tube, installed at Hypervelocity Impact Research Center in Harbin Institute of Technology. One couple of parallel laser light curtains placed at the muzzle of the tube is used to trigger the timing device and then get the exit velocities. The perforation process was photographed and the projectile residual velocity was obtained by a high-speed video camera. The sketch of the experiment set-up is shown in figure 1.

### 2.2. Projectiles and target plates

In this study, the projectiles were made of hardened steel 38CrSi. All projectiles were machined from the original rods with diameter 15 mm to cylinders of a nominal diameter  $D_i = 12.62$  mm and a nominal length  $L_i = 25.4$  mm. In order to satisfy the rigid assumptions, all projectiles were heat treated to quite high strength (the Rockwell hardness 50 HRC or more [10]).

The target plate material is 7A04 aluminum alloy with 3.3 mm thickness and yield stress about 250 MPa. The plates with dimension  $200 \times 200$  mm<sup>2</sup> were clamped in a circular frame by four screws with a free span diameter of 150 mm.

The projectile sketch and target plate installation are presented in figure 2.

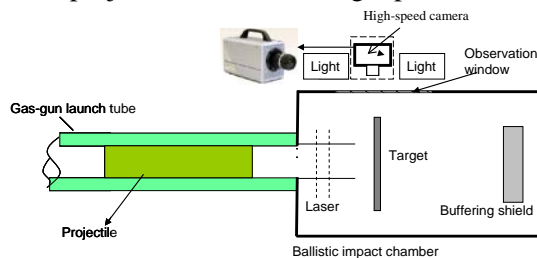


**Figure 1.** Experiment diagrammatic drawing.

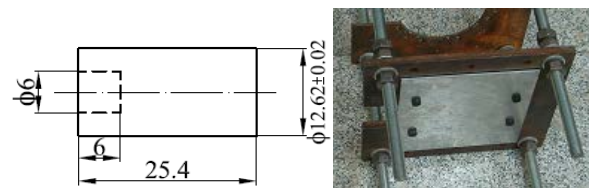


**Figure 2.** The projectile and target plate installation.

### 2.3. Test results

The total 11 impact tests were completed, in which 3 of the target plates were not perforated, and 1 embedded the projectile, however, the remaining 7 were perforated by the projectiles. All of the test results are shown in table 1, where  $m_p$ ,  $v_i$ ,  $v_r$ ,  $h_m$  and  $m_{pl}$  denote projectile mass, initial velocity, residual velocity, target plate maximum deflection and plug mass, respectively.

Some high-speed camera pictures of the perforation process from a typical test with projectile initial velocity 138.5 m/s are shown in figure 3. As seen, an intact plug was rushed out with the projectile perforated the target and no obvious deformation was found on the projectile. In addition, the projectile's attitude was keeping quite well in the whole perforation process.

Initial ( $v_i$ ) and residual ( $v_r$ ) velocities of the projectiles were measured during testing, as shown in figure 4. The velocity in which the projectile inserts the target plate was seen as the ballistic limit velocities  $v_{bl}$ , i.e.,  $v_{bl} = 119.1$  m/s. The line through the data points was determined based on a generalization of an analytical model originally proposed by Recht and Ipson [11]:

$$v_r = a(v_i^p - v_{bl}^p)^{1/p} \quad (1)$$

where  $a$  and  $p$  may be considered as empirical constants. Note that the Recht-Ipson analytical model, with  $a = m_p/(m_p + m_{pl})$ ,  $p = 2$ , is only valid if the plastic deformation of the projectile during impact is negligible, which is the case in these tests.

At the same time, the three constants,  $a$ ,  $p$  and  $v_{bl}$  can be also fitted to the test data by using the method of least squares. Figure 4 shows experimentally ballistic limits obtained, together with assessed values of  $a$  and  $p$  through the above two methods. Confidence intervals of  $a$  and  $p$  with 95%

confidence level are (0.50, 1.40) and (1.11, 2.86), respectively. Even though some spread is seen in the plot, the agreement between the experimental data and the Recht-Ipson model is in general good.

**Table 1.** The test records and results.

#	$m_p$ /(g)	$v_i$ /(m/s)	$v_r$ /(m/s)	$h_m$ /(mm)	$m_{pl}$ /(g)	Remarks
1	23.01	91.4	0	5.22	0	rebound
2	23.01	103.6	0	7.55	0	rebound
3	23.01	108.0	0	8.93	0	rebound
4	23.41	119.1	0	--	0.912	insertion
5	23.01	122.2	10	8.32	0.941	perforation
6	23.10	123.2	40.2	8.20	0.909	perforation
7	23.01	131.2	60.1	8.30	0.903	perforation
8	23.41	132.3	63.5	7.98	0.879	perforation
9	23.01	138.5	53.6	7.73	0.954	perforation
10	23.41	142.9	61.3	7.68	0.958	perforation
11	23.10	164.3	113.4	6.80	0.898	perforation

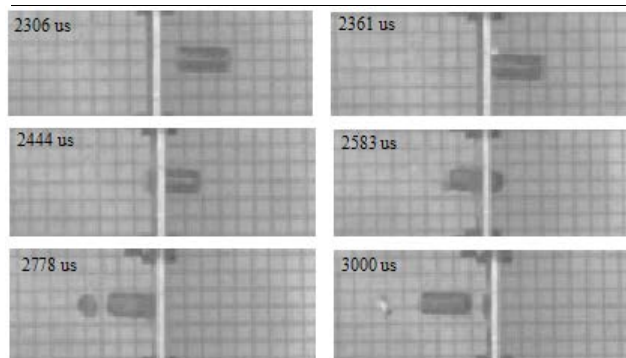


**Figure 3.** Typical perforation process pictures by high-speed camera ( $v_i = 138.5$  m/s,  $v_r = 53.6$  m/s).

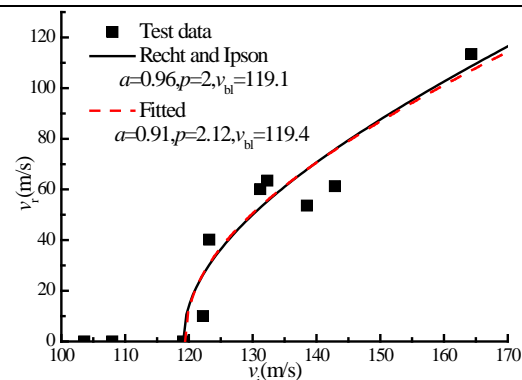


**Figure 4.** The initial versus residual velocity curve by Recht-Ipson model and fitted test data.

Figure 5 shows several typical damaged targets' photos. When the projectile did not perforate the target, an obvious bulge was found in the back of the plate, and when perforate, a round plug and obvious structure deformation was seen.

The target maximum deflection increase with projectile initial velocity in the situation of imperforation, and it reached maximum value near the ballistic limit. However, when target plate is perforated, with the velocity increasing, the maximum deflection value of target plate reduces gradually, as seen in figure 6. Figure 7 showed that several deflection curves of typical targets. As seen, the target deformation is most serious when the velocity is near the ballistic limit.

### 3. Simulation and results

#### 3.1. Finite Element Model and Parameters

All impact tests were analyzed using the ABAQUS/EXPLICIT assuming 2D axisymmetric conditions, and the geometry of the targets and projectiles in the numerical models was identical to that used in the experimental tests. The geometry model and mesh were shown in figure 8. Before the simulation, we firstly confirmed convergence of the model by increasing the numbers of elements doubled.

The material model parameters were obtained by material performance testing and literature [12].

Quasi-static tensile tests were carried out using plate specimen with a gauge length of about 30 mm and cross-section dimensions  $10 \times 3.3 \text{ mm}^2$ , as shown in figure 9, at a nominal strain rate of  $1.11 \times 10^{-3} \text{ s}^{-1}$  in an INSTRON 5569 universal testing machine.

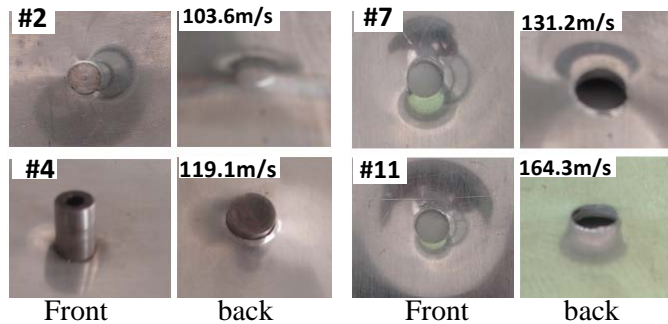


**Figure 5.** Several typical target deformation forms after impact.

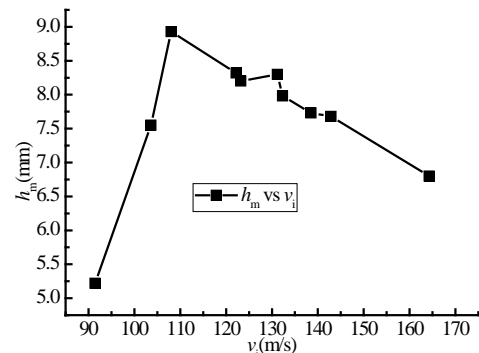


**Figure 6.** The relationship of target maximum deflection and projectile initial velocity.

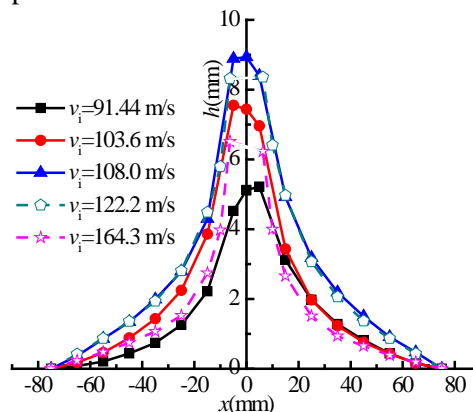


**Figure 7.** Several typical target plates' deflection curves in the back

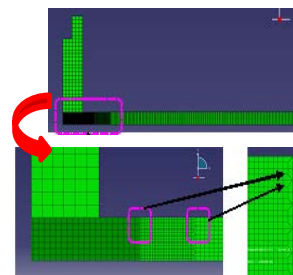


**Figure 8.** The geometry model of of quasi-static tensile simulation.

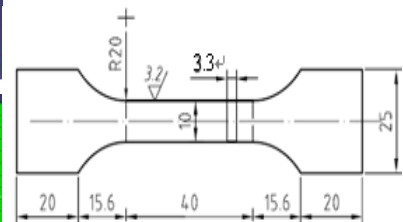


**Figure 9.** The shape and sizes of quasi-static tensile specimen.

A modified version of the Johnson-Cook constitutive relation was chosen as a first approach in order to model the target material based on the Quasi-static tensile test results. Here, the equivalent stress is expressed as [12]:

$$\begin{cases} \sigma_{eq} = A + A_1[1 - \exp(-\varepsilon_{eq}/t_1)] + A_2[1 - \exp(-\varepsilon_{eq}/t_2)], & \varepsilon_{eq} < (\varepsilon_u - A/E) \\ \sigma_{eq} = \sigma_u[w(1 + \varepsilon_{eq} - \varepsilon_u + A/E) + (1-w)(\varepsilon_{eq}/\varepsilon_u)^{\varepsilon_u}], & \varepsilon_{eq} \geq (\varepsilon_u - A/E) \end{cases} \quad (2)$$

The meaning of every constant is same as literature [12].

Figure 10 compares the numerically obtained load-elongation curve by using the proposed strain hardening term with the test result. As seen, the modified model can give close prediction.

The strain rate hardening term and temperature softening term with corresponding parameters are same as literature [12].

Failure is modeled using a fracture criterion proposed by Cockcroft and Latham (CL) where it is assumed that fracture depends on the stresses imposed as well as on the strains developed [4]. The model is expressed as:

$$W_1 = \int_0^{\varepsilon_{eq}} \langle \sigma_1 \rangle d\varepsilon_{eq} \quad (3)$$

where if  $\sigma_1 \geq 0$ ,  $\langle \sigma_1 \rangle = \sigma_1$ ; otherwise,  $\langle \sigma_1 \rangle = 0$ . Here  $\sigma_1$  is the first principal stress. When  $\varepsilon_{eq}$  reaches  $\varepsilon_f$ ,  $W_1 = W_{cr}$ , the material failure will occur.

All parameters used in impact simulation were listed in table 2.

**Table 2.** All material parameters used in simulation.

$E(\text{GPa})$	$\nu$	$\rho(\text{kg/m}^3)$	$C_p(\text{J/kgK})$	$T_r(\text{K})$	$T_m(\text{K})$	$m$
69.35	0.31	2850	921	293	878	1.015
$\chi$	$A(\text{MPa})$	$\sigma_u(\text{MPa})$	$\varepsilon_u$	$A_1(\text{MPa})$	$t_1$	$A_2(\text{MPa})$
0.9	251.2	299	0.0275	50.2	0.022	11.8
$t_2$	$w$	$\dot{\varepsilon}_0(\text{/s})$	$C$	$W_{cr}(\text{MPa})$		
0.0023	0	0.0011	0.014	125		

### 3.2. Simulation Results

Figure 11 shows a typical perforation process at the velocity of 122.2 m/s. As seen, it is very similar to experiment (see figure 3). The initial-residual velocity relationship with simulations and tests was compared in figure 12. The prediction for the ballistic limit almost uniform with the test results. When velocity is away from the ballistic limit velocity, there are some differences between simulation and experiment results. The reason may be that there are some differences between some of reference material parameters and the material used here. Even so, the numerical simulation can still reflect the trend of the test.

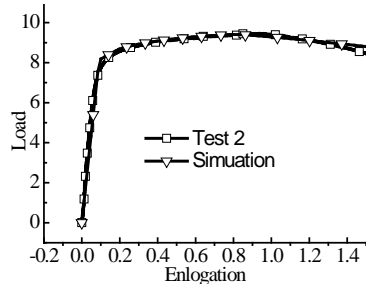


**Figure 10.** Comparison of load-elongation curve between the test and the proposed model

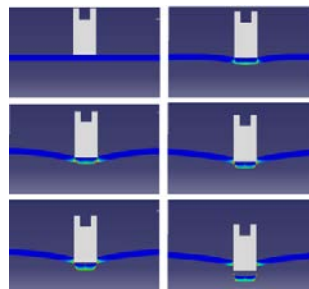


**Figure 11.** A typical perforation process of simulation ( $v = 122.2$  m/s).

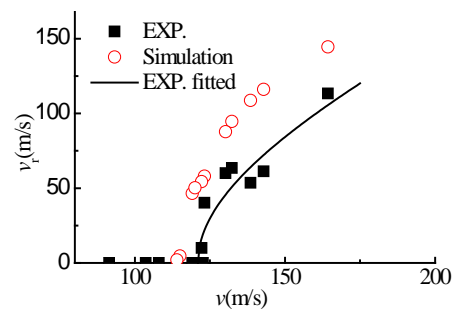


**Figure 12.** Comparison of the initial-residual velocity data between the tests and the numerical simulations.

The stress triaxiality ratio  $\sigma^*$  is defined as  $\sigma^* = \sigma_H / \sigma_{eq}$ , where  $\sigma_H$  is hydrostatic stress and  $\sigma_{eq}$  is equivalent stress. Different  $\sigma^*$  value indicates different element stress state in simulation, i.e., when  $\sigma^* \leq -1/3$ , the element suffers compression stress state; when  $-1/3 < \sigma^* < 0$ , the element stress is a combination state of compression and shear; when  $\sigma^* = 0$ , the stress state is pure shear; when  $0 < \sigma^* < 1/3$ , a combination state of tension and shear happens; when  $\sigma^* \geq 1/3$ , the element stress state becomes tension, where a state of uniaxial tension turns up when  $\sigma^* = 1/3$  just right.

To learn target plates' failure mechanisms, details from simulations are extracted. Figure 13 gives the stress triaxiality and damage accumulation history of several typical failed elements in front, center, and back of the target plate at impact velocity of 122.2 m/s. When the damage indicator of an element reaches 1, the element failed completely. As seen, only the element in front suffers compression-shear and tension-shear stress states in the process of damage accumulation; while tension is the most major contribution to damage accumulation in the two elements of center and back. The same treatment was also done for other simulations, which are no longer shown here. From the above, tension stress state is the main reason of target plate failure.



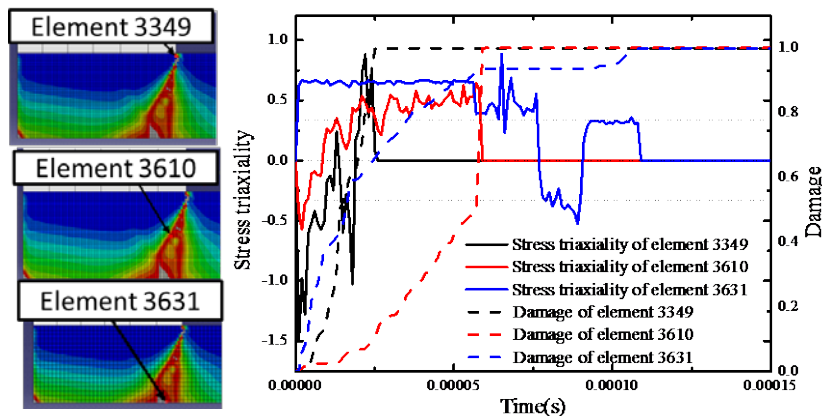


**Figure 13.** History of the stress triaxiality and damage indicator in several typical target failed elements at  $v_i = 122.2$  m/s.

#### 4. Conclusion

The ballistic resistance of 7A04 aluminum alloy plates with 3.3 mm thickness against blunt high strength steel projectiles with 12.7 mm diameter has been investigated by lab-scale ballistic test and finite element simulation. The ballistic limit velocity was obtained and plugging failure and obvious structure deformation of targets were observed. The deformation is most serious in ballistic limit velocity. The valid simulation results were obtained by 2D numerical simulations using ABAQUS/EXPLICIT combined with material performance testing. Detailed computational results extracted in simulations have proven that the tension stress state is the most major reason that leads to target plates' failure mainly when perforated.

#### References

- [1] Hatch J E 1984 *Aluminium: properties and physical metallurgy* (Metals Park Ohio: American Society for Metals)
- [2] Forrestal M J, Luk V K, Rosenberg Z and Brar N S 1992 Penetration of 7075-T651 aluminum targets with ogival-nose projectiles *Int. J. Solids Struct.* **29** 1729-36
- [3] Demir T, Ubeyli M and Yildirim R O 2008 Investigation on the ballistic impact behavior of various alloys against 7.62 mm armor piercing projectile *Mater. Design* **29** 2009-16
- [4] Børvik T, Hopperstada O S and Pedersena K O 2010 Quasi-brittle fracture during structural impact of AA7075-T651 aluminium plates *Int. J. Impact Eng.* **35** 537-51
- [5] Piekutowski A J, Forrestal M J, Poormon K L and Warren T L 1996 Perforation of aluminum plates with ogive-nose steel rods at normal and oblique impacts *Int. J. Impact Eng.* **18** 877-87
- [6] Børvik T, Clausen A H, Hopperstad O S and Langseth M 2004 Perforation of AA5083-H116 aluminium plates with conical-nose steel projectiles-experimental study *Int. J. Impact Eng.* **30** 367-84
- [7] Gupta N K, Iqbal M A and Sekhon G S 2006 Experimental and numerical studies on the behavior of thin aluminum plates subjected to impact by blunt-and hemispherical-nosed projectiles *Int. J. Impact Eng.* **32** 1921-44
- [8] Gupta N K, Iqbal M A and Sekhon G S 2007 Effect of projectile nose shape, impact velocity and target thickness on deformation behavior of aluminum plates *Int. J. Solids Struct.* **44** 3411-39
- [9] Børvik T, et al. 2009 Perforation of AA5083-H116 aluminium plates with conical-nose steel projectiles-calculations *Int. J. Impact Eng.* **36** 426-37
- [10] Xiao X, Zhang W, Wei G and Mu Z 2010 Effect of projectile hardness on deformation and fracture behavior in the Taylor impact test *Mater. Design* **31** 4913-20
- [11] Recht R F and Ipson T W 1963 Ballistic perforation dynamics *J. Appl. Mech.* **30** 384-90
- [12] Xiao X, et al. 2011 Experimental and numerical investigation on the deformation and failure behavior in the Taylor test *Mater. Design* **32** 2663-74